Ridge Localizations and Networks in Thin Films Compressed by the Incremental Release of a Large Equi-biaxial Pre-stretch in the Substrate

Atsushi Takei, Lihua Jin, John W. Hutchinson, and Hiroyuki Fujita*

The intriguing buckling patterns exhibited by bilayer systems composed of a thin stiff film bonded to a thick elastomeric substrate have been studied extensively in recent years both experimentally and theoretically. Under compression, the film is constrained by the substrate and buckles with a wavelength that is usually large compared to the film thickness, yet small compared to the substrate thickness. The most common patterns observed are the sinusoidal wrinkle mode when compression in one direction is dominant,[1] and the herringbone[2,3] and labyrinth[2–4] modes when compression is equi-biaxial. The present paper is part of the ongoing research effort in the soft-materials community to produce and manipulate specific buckling patterns.[5,6] Most of the previous work has focused on buckling patterns of bilayer systems under small compression. Recent work, however, has demonstrated that large compression of a bilayer system can engender other surface patterns such as period-doubling[7] and folding,[8,9] opening the way for the creation of a wider array of surface patterns. These post-wrinkling modes involve the large strain behavior of the substrate and geometrical non-linearity of the films in an essential way.

The focus of the present paper is on the most recent of the post-wrinkling modes to be discovered, the ridge localization mode. While folds and creases protrude into the substrate, the ridge is a large amplitude localization that pushes out from the substrate. This mode should be characterized as a localization because the large amplitude of the ridge is fed by flattening the nearby wrinkle undulations resulting in ridges that are separated from each other by expanses of relatively flat film. Thus, a distinct feature of the transition from wrinkles to ridges is the abrupt increase of spacing from crest to crest. The ridge localization was predicted to occur,[10] and has been observed experimentally,[5,6,11] only when a relatively large pre-stretch was imposed on the elastomeric substrate prior to film attachment. Controlled incremental release of the pre-stretch of the thick substrate then imposes compression on the film, which drives buckling. The large substrate pre-stretch favors the formation of the ridge mode.[10] The buckling pattern reported in this paper consists of localized ridge lines separated by relatively flat patches of film. Exploitation of a high pre-stretch produces these new high aspect convex structures that have the potential for expanding the range of surface morphologies for applications, such as in the fields of smart adhesion,[12] hydrophobic surfaces,[13–15] and templates for micro-patterning.[16] The present paper features a method for applying an equi-biaxial pre-stretch and release, and thereby complements recent related work on ridge formation that has primarily been limited to uni-axial or plane strain pre-stretch.[5,10,11,17] This paper also highlights the underlying characteristics and nature of ridges, including emergence and evolution aspects that remain unclear due to the highly non-linear behavior of the system caused by high pre-stretch. For the system and approach employed here, delamination[5,18,19] and cracking[20] of the thin film, which often accompany wrinkling instabilities, have been avoided.

Thus, in this paper, the transition to the ridge buckling morphology is studied in a bilayer system comprising a thin stiff film attached to a relatively thick compliant substrate. The substrate is subject to a large equi-biaxial pre-stretch prior to film attachment, and then the bilayer is incrementally unloaded producing equi-biaxial compression in the film. The experiments are carried out using a specially designed micro-fluidic loading system. The system enables equi-biaxial pre-stretch and incremental compression simply by changing pressure inside the micro-fluidic chamber (as used previously in the literature[21]), while more conventional loading systems[3,6] require well-synchronized control of mechanical stretchers. Because mechanical stretchers are not employed, our method can simultaneously handle several systems at a scale of 1 cm within the film deposition cavity, whose space is often limited. Using this system, we clearly captured transitions from wrinkles to localized ridges and the formation of a ridge network surrounding flattened regions. In particular, the experiments reveal the evolution of the ridge structure, which involves propagation of individual ridges to form a network. The influence on the geometry of the ridge is explored by varying the pre-stretch and the thickness of the thin film. Further, finite element simulations have been carried out to obtain conditions for the localized ridge formation and propagation. Unlike sinusoidal or herringbone wrinkles, the ridge is a finite amplitude mode, and the wrinkle-to-ridge transition is subcritical, as described more fully in conjunction with the simulations. As the pre-stretch is released, once a ridge forms, it grows and saturates to a height comparable to its width.

Figure 1a illustrates the method of preparing the highly pre-stretched substrate. A chamber capped by a flat layer of the

Dr. A. Takei, Prof. H. Fujita
Institute of Industrial Science
The University of Tokyo
4–6–1 Komaba, Meguro-ku, Tokyo 153–8505, Japan
E-mail: atakei@iis.u-tokyo.ac.jp
L. Jin, Prof. J. W. Hutchinson
School of Engineering and Applied Sciences
Kavli Institute
Harvard University
29 Oxford Street, Cambridge, MA 02138, USA

DOI: 10.1002/adma.201306162

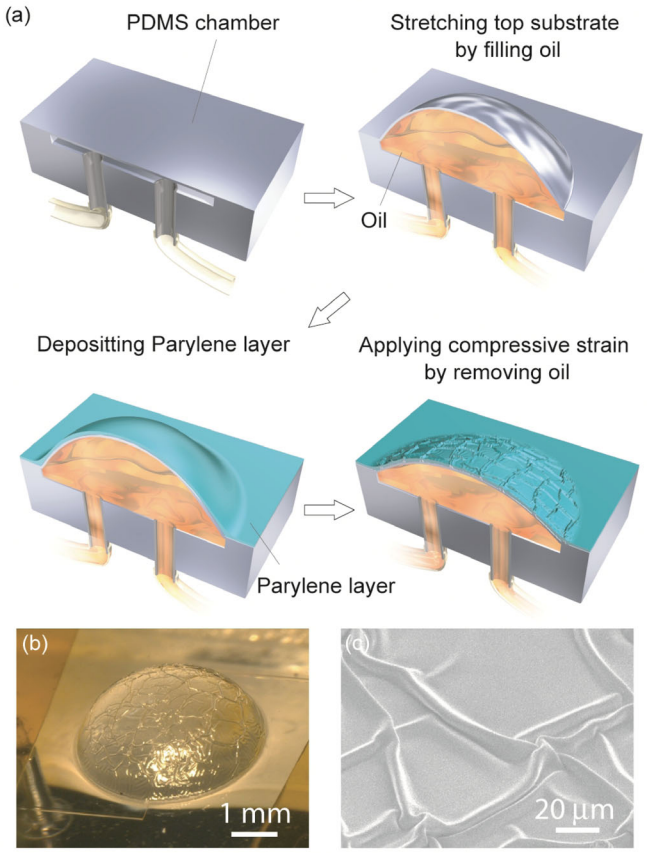

Figure 1. a) Schematic illustration showing the preparation of the highly pre-stretched bilayer system using micro-fluidics. b) Image of the experimental set-up: Compressive strain is applied by reducing the oil inside the chamber, and a ridge structure emerges on the surface. c) SEM image of the ridge structure: The localized convex structure is observed concomitantly with a flattening of the neighboring film surface.

elastomeric substrate material, polydimethylesiloxane (PDMS), is formed. The substrate layer is then stretched by filling the chamber with oil. With the pressure inside the chamber held constant, an organic polymer material, Parylene-C, is deposited on the surface to form the film. Prior to deformation, the PDMS substrate layer has a thickness in the range of h_s = 50–300 μm and a shear modulus of $\mu_s \approx 0.33$ MPa. The Parylene film (thickness, h_f: 85 nm to 1.3 μm; shear modulus $\mu_f \approx$ 0.58 GPa) is stress-free as deposited. The stress–strain curves of PDMS and Parylene as well as the fabrication details are given in Figure S1 in the Supporting Information. The equi-biaxial pre-stretch λ_0 attained in the central region of the substrate is defined as the ratio of the length after stretch L to the original length L_0, $\lambda_0 = L/L_0$. An equi-biaxial compressive strain, ε, is exerted on the film in the central region when oil is released incrementally from the chamber. The compressive strain is defined as $\varepsilon = 1 - l/L$, where the current length is l. Compared to methods such as thermal expansion[4] and swelling[2,22–24] for inducing equi-biaxial strain, the present method can induce a pre-stretch greater than 1.5, and the magnitude of the pre-stretch can be readily adjusted by controlling the pressure inside the chamber. The thickness of the substrate is selected to be at least 50 times that of the film, and the film is about 2000 times stiffer than the substrate. The radius of the chamber is 2 mm, and the effect on the instability due to the curvature of the chamber is considered to be negligible (discussed further in the Supporting Information). Figure 1b and c show the typical morphology of the surface with ridges. Figure 1b shows an overview of an experimental set-up taken by a microscope at a point in the release process where the ridges have formed with the chamber still substantially inflated. Figure 1c shows an scanning electron microscopy (SEM) image of the surface of another sample. This figure reveals localized ridges separated by extensive unbuckled regions. Unlike a typical wrinkle or herringbone buckling pattern,[2,3] which fills the entire surface of the film, the deformation producing a ridge is localized with extensive regions on both sides of the ridge being almost flat. Furthermore, unlike creases and folds[8,9] which protrude into the substrate, ridges push upward from the substrate. These and other aspects of the ridge mode will be discussed in further detail later in the paper. The scale of the ridges depends on the film thickness h_f. In Figure 1b, with $h_f \approx 1$ μm, the width of the ridges is ~50 μm, while in Figure 1c, with $h_f \approx 100$ nm, the width of the ridges is ca. 5 μm. In neither of these cases has the Parylene thin film delaminated from the PDMS substrate (a cross-sectional view is available in Figure S2 in the Supporting Information). The pre-stretch and compressive strain in the central region are estimated by measuring the height of the chamber at each stage of inflation or deflation, and the non-uniformity of the pre-stretch of the system is considered to be negligible; see Figure S3 in the Supporting Information for more details.

An overview description of one particular experiment is now presented. As the equi-biaxial compression in the film is increased by slowly releasing oil from the chamber, wrinkles first form, and then, with further compression, wrinkles give way to ridges as seen in **Figure 2**. In this experiment, h_f = 100 nm, h_s = 50 μm, and the substrate has been pre-stretched to $\lambda_0 = 1.59$. For this system, dimpled wrinkles, reflecting the equi-biaxial compressive stress experienced by the film, cover the surface at $\varepsilon \cong 0.05$ (Figure 2a,b). As the compressive strain experienced by the film is further increased, the dimples become more like wrinkles (Figure 2c), and then, by $\varepsilon = 0.066$, the transition to ridge-like features is evident (Figure 2d,e). At $\varepsilon = 0.066$, ridges are observed to advance flattening neighboring regions under conditions when no oil is released from the chamber such that the overall compression in the system is nominally fixed (Figure 2f). As will be shown later, the critical compressive strain for ridge formation is only slightly above that for the wrinkle pattern, and in the present study, it has not been possible to experimentally resolve the difference between the two critical strains.

Further experimental details on the development and evolution of a ridge network are presented in **Figure 3**. For this experiment, the substrate is pre-stretched to a larger value, $\lambda_0 = 1.85$, enhancing ridge formation and the ensuing ridge network. In this case, h_f = 85 nm and h_s = 50 μm. As shown in Figure 3a, unconnected ridges are first formed with wrinkles appearing perpendicular to the ridges. With the increase of compression, new ridges nucleate and propagate perpendicularly to existing ones until they become blocked by a pre-existing ridge (Figure 3b,c). A network of ridges is created; the few wrinkles

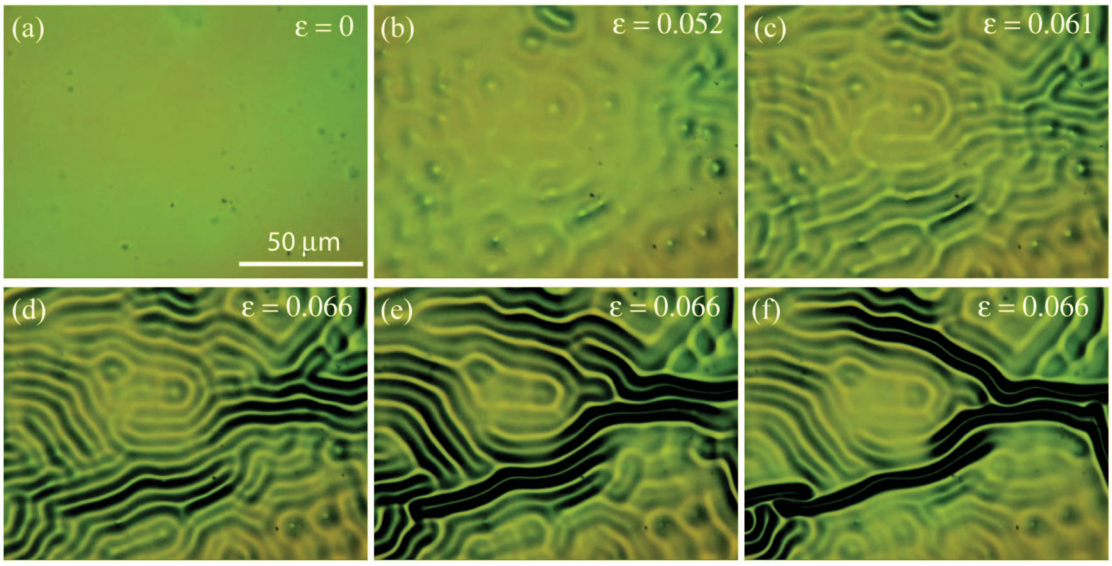

Figure 2. Wrinkle-to-ridge transition. a) In its initial state, the surface of the chamber is flat. b) With compressive strain, the dimpled wrinkle pattern is engendered on the surface. c) With increasing compressive strain, the dimpled wrinkle pattern transforms into the wrinkle pattern. d) With further compression, some peaks of the wrinkles increase their height and ridges nucleate. e,f) Under essentially the same applied compression, ridges can propagate and flatten neighboring surfaces.

still present illustrate clearly the distinction between wrinkles and ridges. With a further increase in compression, the network grows denser (Figure 3d,e) until there is no space for new ridges to be nucleated and the network saturates (Figure 3f). The evolution seen here for the ridge pattern is similar to the evolution of folds in a compressive bilayer without pre-stretch.[8]

The dependence of the geometry of the ridge and the threshold pre-stretch λ_c required for the formation of a ridge was measured using systems with seven different thicknesses of the Parylene film, ranging from h_f = 85 nm (with h_s = 50 μm) to h_f = 1.3 μm (with h_s = 300 μm). For a given pre-stretch, λ_0, the compressive strain ε is increased by the release of the pre-stretch, and the surface of the bilayer is carefully examined in order to see the buckling patterns that emerge and, in particular, whether ridges form. The wrinkle/ridge phase diagram is plotted in Figure 3g. The threshold pre-stretch is approximately $\lambda_c = 1.4$ for ridge formation — that is, for smaller pre-stretches, ridges are not observed, and for larger pre-stretches, they are observed. The threshold appears to be independent of the thickness of the stiff film, consistent with what is expected on dimensional grounds for thick substrates. For cases in which ridges are formed, the width w and the height A of the ridges (as defined in the inset of Figure 3h) are also measured and plotted in Figure 3g. The measurements presented in Figure 3h have been taken for the cases in Figure 3g, in which the pre-stretch λ_0 was between 1.4 and 1.6. The width w is proportional to the film thickness h_f, and for the stiffness ratio of the present film/substrate system, the experimental results are fitted using $w = 34h_f$. If one imagines a ridge to be the localization of a single wrinkle, one would expect the ridge width w to be on the same order of magnitude as the wavelength of the wrinkle l_w. In an earlier report,[10] the wavelength of a wrinkled linear elastic film on a neo-Hookean substrate subject to an equi-biaxial pre-stretch λ_0 is $l_w = 2\pi h_f \left(2\mu_f \lambda_0 / \left(3\mu_s(1+\lambda_0^3)\right)\right)^{1/3}$. With μ_f/μ_s = 1750 and $\lambda_0 = 1.5$, one finds $l_w = 46h_f$, which is on the same order of magnitude of the experimentally measured wavelength in Figure 3h. In all of these cases, the ratio of the ridge height A to its width w, A/w (Figure 3h, inset) is significantly larger than the amplitude/wavelength ratio of the conventional wrinkle at these compressive strains, i.e., ~0.1.

Numerical simulations employing the commercial finite element software, ABAQUS, were carried out to study and quantify the conditions for ridge formation. These simulations go well beyond the initial plane strain studies[10] where ridges were first discovered theoretically. In addition to systematically exploring the effect of the equi-biaxial pre-stretch on ridge formation, we investigated the mechanics by which the ridges propagate. Simulation details can be found in the Supporting Information, and a detailed paper on the mechanics of ridge formation and propagation will be published at a later date. To break the translational symmetry of the flat surface and initiate wrinkles, a very small initial imperfection in the form of a slight surface waviness is introduced. The formation of wrinkles and ridges is simulated under a generalized plane strain condition in the 1–2 plane (as defined in **Figure 4**a) with an equi-biaxial pre-stretch λ_0 in the substrate and with the subsequent equi-biaxial compressive strain ε applied to both film and substrate. In keeping with generalized plane strain, the overall strains in the 1–3 directions are equi-biaxial, but the displacements caused by the wrinkles or by the ridges relative to the equi-biaxial state are subject to the constraint of plane strain. The plane strain constraint limits wrinkling and ridging to 1D entities — the dimple mode seen in Figure 2 and the 2D ridge pattern in Figure 3 are excluded. Nevertheless, the essence of ridge formation is captured within the constraint adopted. Both film and substrate are modeled as incompressible neo-Hookean materials. Ridges grow at the expense of neighboring wrinkles, and therefore, to simulate ridge localization the width of the

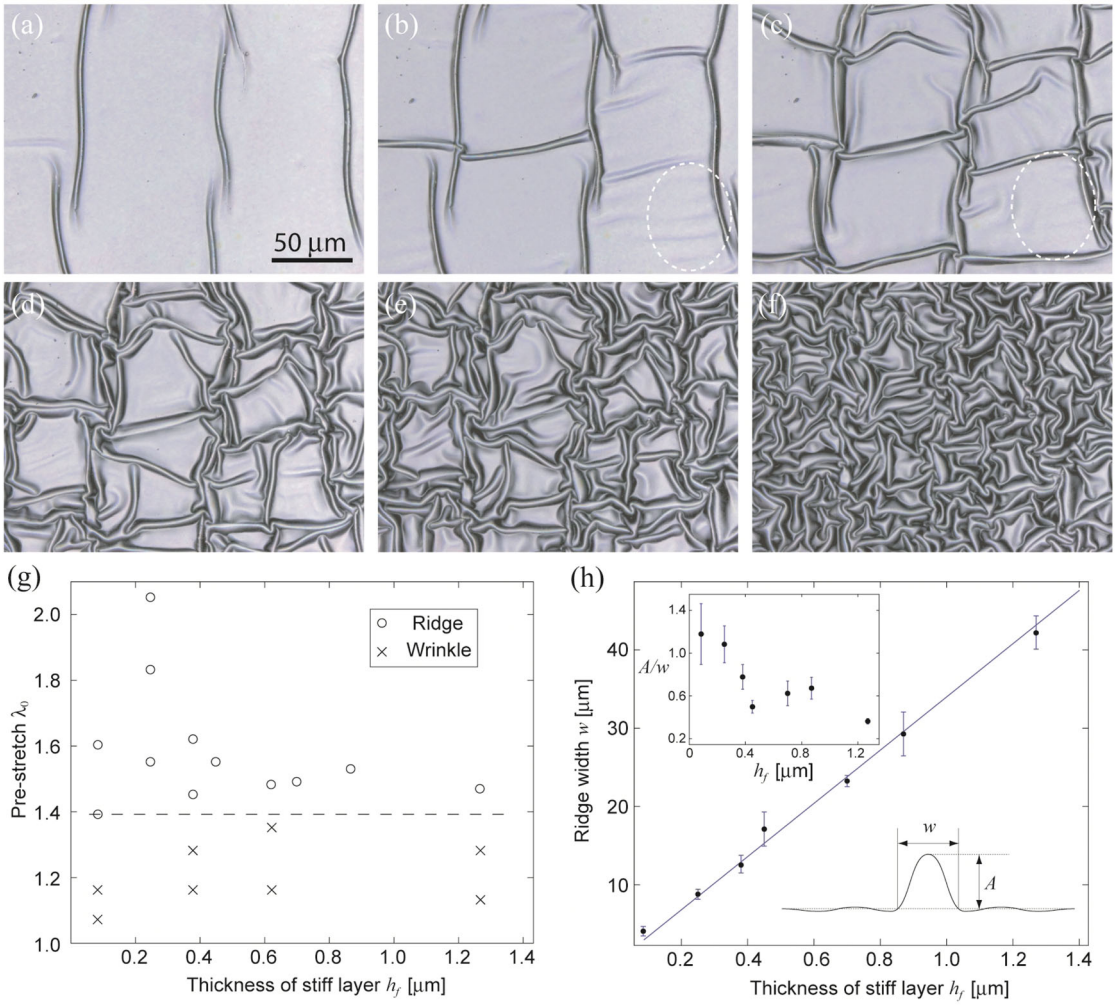

Figure 3. The formation of the ridge network. a) Upon compression, unconnected ridges first appear. b,c) With increasing compression, new ridges nucleate perpendicular to the existing ridges. As marked with the dashed circles, wrinkled regions emerge before ridge nucleation, and they become flattened after the formation of the ridge. d,e) With even further increases in the compression, the network grows denser, and finally, f) it is completely packed. g) Phase diagram of the wrinkle/ridge mode. Ridge structure appears with the pre-stretch of $\lambda_0 > 1.4$. h) Relationship between stiff film thickness and width of the ridge. Fitting curve is $w = 34h_f$. Inset: Relationship between height/width ratio, A/w, of a ridge and the stiff film thickness h_f is embedded.

computational model must be at least several times the wrinkle wavelength. In the present simulation, this width is $L \cong 10l_w$. By making use of symmetry, only half of this length is simulated, and as shown in Figure 4a, the symmetric condition is set at the left boundary.

When ε reaches a critical strain denoted by ε_w, wrinkles start to form in the one direction with wavelength l_w. The computed values of ε_w and l_w are in close agreement with predictions of the classical bifurcation results for wrinkling.[10] As the applied compression is further increased, the wrinkle amplitudes increase, but the nominal wrinkle wavelength does not change.

We found that the wrinkle-to-ridge transition is unstable (subcritical in the language of bifurcation theory), such that a wrinkle snaps dynamically to a ridge with a much larger amplitude. Conventional quasi-static simulations fail for such phenomena, and special numerical techniques are required, such as the arc-length method[25,26] or dynamic simulations. We developed the following quasi-static technique to probe for the existence of a ridge and found it to be systematic and reliable. As depicted in Figure 4a, under the fixed overall strain ε, an additional vertical displacement Δ is imposed on the peak of the wrinkle at the left boundary. The associated reaction force $F(\Delta)$ is computed. The system remains stable when the additional vertical displacement Δ is prescribed, and this allows large displacement equilibrium states to be discovered wherever $F = 0$. If a state with $F = 0$ is found when Δ is non-zero, then that state can exist (without an external force) at the strain ε although it may be stable or unstable. An example of this process is shown in Figure 4b. The ridge seen in Figure 4b (at $F = 0$) is clearly a localized mode in a sense that the amplitudes of the wrinkles neighboring it have diminished significantly.

Figure 4c–e show the F–Δ relationship under different fixed strains ε for three pre-stretches, λ_0 =1.2, 1.4, and 1.6, in the substrate. The shear modulus ratio of the film to the substrate μ_f/μ_s

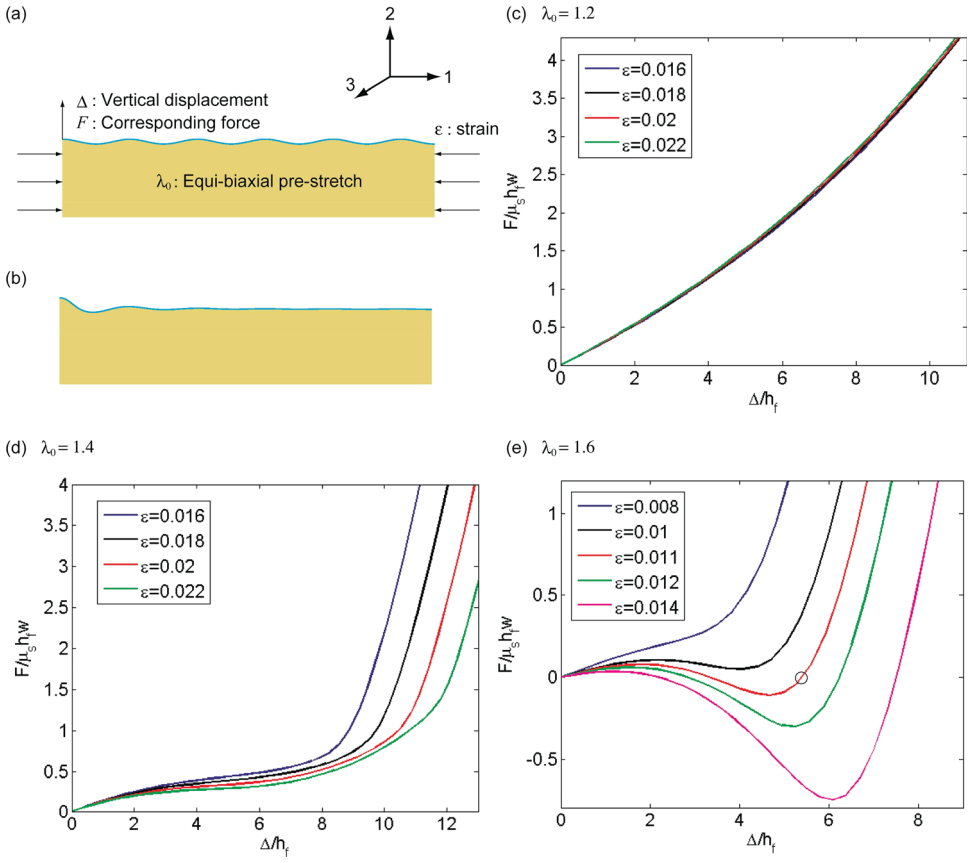

Figure 4. Finite element simulation results. a) Simulation showing wrinkles under an equi-biaxial strain of $\varepsilon = 0.011$ and a pre-stretch of $\lambda_0 = 1.6$ in the substrate. b) Simulation showing the large amplitude ridge state under the same loading condition as in (a). In (a) and (b), the blue line represents the thin film, and the yellow–brown area represents the substrate. c–e) F–Δ curves are obtained for various fixed strains for an equi-biaxial pre-stretch of $\lambda_0 =$ 1.2 (c), 1.4 (d), and 1.6 (e) with $\mu_f/\mu_s = 2000$ and $(h_f + h_s)/h_f = 50$.

has been taken to be 2000, slightly larger than that of the experimental system for simplicity, and the thickness ratio of the bilayer to the film is set to be 50 so that the substrate can be considered much thicker than the film. When $\lambda_0 = 1.2$, the critical condition for wrinkle initiation is approximately $\varepsilon_w \cong 0.0022$. As shown in Figure 4c, when the strain ε is fixed at 0.016, F sharply increases with Δ, and F does not become zero. In fact, for all of the fixed strains ε, from 0.016 to 0.022, the F–Δ curves almost overlap. The behavior for a larger pre-stretch, $\lambda_0 = 1.6$, is dramatically different. For small applied compression, $\varepsilon = 0.008$, F increases monotonically with Δ (Figure 4e). However, for larger ε, the F–Δ curves become non-monotonic: F increases, decreases, and then increases again with Δ. Above a critical ε, the F–Δ curve intersects the Δ-axis at three points: the origin, which represents the wrinkle state; the middle point, which represents an unstable medium amplitude ridge; and the point on the right, which represents a stable large amplitude ridge. This plot clearly shows the large amplitude nature of ridges. Figure 4a shows the simulation result of wrinkles for $\varepsilon = 0.011$ when $\lambda_0 = 1.6$. Figure 4b shows the simulation result for the stable large amplitude ridge for the same strain and pre-stretch (as indicated by a circle in Figure 4e). The additional film length needed to form the ridge is obtained by flattening neighboring wrinkles, and it is this feature which gives rise to localization. At the intermediate pre-stretch, $\lambda_0 = 1.4$, the F–Δ relation is strongly non-linear. However, even at $\varepsilon = 0.03$ (not shown in Figure 4d), F does not become zero at non-zero Δ. To conclude, our simulations suggest that the threshold value of the pre-stretch required for ridges to form is slightly larger than $\lambda_0 = 1.4$. This is in general agreement with the experimental observations reported in Figure 3g.

Additional simulations were performed to show the evolution of the ridges by a pseudo-dynamic simulation (**Figure 5**). Again, an initial imperfection consisting of a slight waviness is introduced to trigger the initiation of the wrinkles. The bilayer is loaded equi-biaxially with an equi-biaxial pre-stretch $\lambda_0 = 1.6$ in the substrate. The modulus ratio and thickness ratio are the same as that used in for Figure 4. With a gradual compression increase, well-defined wrinkles first form. When the compression ε increases to about 0.0185, a ridge initiates and snaps to a state with finite amplitude. As noted earlier, the ridge forms at the expense of neighboring wrinkles. The ridge quickly grows to a saturated height when ε reaches around 0.0205. With the further increase of compression, more ridges form. However, the height of previously formed ridges changes relatively little with increasing compression, which is consistent with the notion of a saturated height. For $\varepsilon = 0.1163$, the ratio of the height of the ridges to the film thickness predicted for this system is

ADVANCED MATERIALS
www.advmat.de

www.MaterialsViews.com

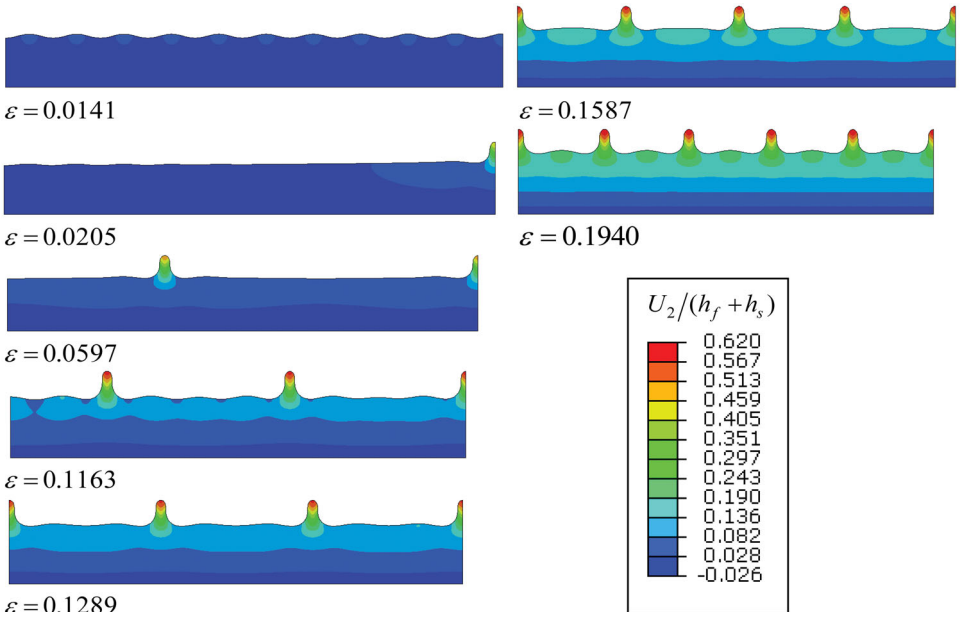

Figure 5. Evolution of the morphology of the film–substrate bilayer at different equi-biaxial strains ε, revealing the progression to wrinkles and then to ridges. The scale represents the normalized vertical displacement, $U_2/(h_f+h_s)$. The parameters used in the simulation are as followings: $\lambda_0 = 1.6$, $\mu_f/\mu_s = 2000$, and $(h_f+h_s)/h_f = 50$.

around $A/h_f = 24$, and the ratio of the width of the ridges to the nominal film thickness is around $w/h_f = 29$, such that $A/w = 0.83$. These characteristic length scales of the ridges and the evolution of their behavior predicted by simulations are in reasonable general agreement with the experiments. The experimentally measured width-to-film-thickness ratio in Figure 3h is about 15% higher than the prediction. While the theoretical height-to-thickness ratio is within the range of the experimental results in Figure 3h, the experimental measurements display considerably more variation. In part, this can be explained by the fact that there is some dependence of the ridge amplitude on the applied strain after it is formed. In addition, there may be some influence of the finite thickness of the substrate on A/w; it is not accounted for in the numerical simulations because the height of the ridge is comparable to the substrate thickness in the experiment. The main discrepancy between simulation and experiment is the critical strain for the initiation of wrinkles and ridges — simulations predict somewhat lower critical strains than those measured experimentally. In previous work,[27] residual stress in Parylene film has been noted. For the present system, the residual tensile strain in the Parylene film on the PDMS substrate was measured as ca. 1% (Supporting Information, Figure S4). The applied compression ε has to overcome any residual tensile strain in the film, and it is believed that this accounts for the discrepancy mentioned above.

To summarize, the evolution of the buckling patterns of bilayer film–substrate systems was studied for systems having a large equi-biaxial pre-stretch in the substrate. A micro-fluidics chamber was designed for carrying out the experiments. The pre-stretch in the substrate is tuned by varying the volume of the oil in the PDMS chamber, and compressive strain is applied to the bilayer system by diminishing the volume of oil. Transitions from wrinkles to ridges and the formation and evolution of ridge networks are clearly captured. Ridges are a highly localized deformation mode resulting in the flattening of the film in its vicinity. Details of ridge formation and geometry were studied by varying the pre-stretch and the thickness of the thin film. Finite element simulations were carried out to reveal the highly non-linear character of the ridges and to quantify the conditions for their formation. The wrinkle-to-ridge transition is unstable, or subcritical, and the ridge amplitudes are much larger than those of the wrinkles. The simulations qualitatively capture the experimental results in all respects, and they reproduce most aspects quantitatively with reasonable success. The ability of the present system to attain a high pre-stretch enriches the scope for exploring surface instability patterns of bilayer systems. The ridge mode has higher aspect ratios than the wrinkle mode, and a ridge network consists of isolated patches of flat surface surrounded by ridges. It is hoped that our method will open a new route for creating and improving the properties of functional surfaces, such as hydrophobicity, adhesion, and micro-patterning.

Experimental Section

Surface Transition and Ridge Evolution: In the experiment for Figure 2, the compressive strain is slowly applied by reducing the oil at a rate of 1 μL/min from the PDMS chamber. The surface is observed with a conventional optical microscope. The focal plane of the microscope is set at the summit of the chamber during the process. In the experiment for Figure 3, the surface is observed with an optical surface measurement system that contains a microscope and a laser profiler (Keyence, VK-8710). Image processing software in the system improves the optical images by cancelling the gap of the focal plane induced by the curvature.

Supporting Information

Supporting Information is available from the Wiley Online Library or from the author.

Acknowledgements

The authors acknowledge Prof. Yanping Cao at Tsinghua University for a discussion on simulating ridges. This work was partially supported by a Grant-in-Aid for JSPS Fellows.

Received: December 18, 2013
Revised: February 24, 2014
Published online: March 31, 2014

[1] C. M. Stafford, C. Harrison, K. L. Beers, A. Karim, E. J. Amis, M. R. Vanlandingham, H. C. Kim, W. Volksen, R. D. Miller, E. E. Simonyi, *Nat. Mater.* **2004**, *3*, 545.
[2] S. Cai, D. Breid, A. J. Crosby, Z. Suo, J. W. Hutchinson, *J. Mech. Phys. Solids* **2011**, *59*, 1094.
[3] P. C. Lin, S. Yang, *Appl. Phys. Lett.* **2007**, *90*, 241903.
[4] N. Bowden, S. Brittain, A. G. Evans, J. W. Hutchinson, G. M. Whitesides, *Nature* **1998**, *393*, 146.
[5] Q. Wang, X. Zhao, *J. Appl. Mech.*, **2013**, *1*, 051004.
[6] C. Cao, H. F. Chan, J. Zang, K. W. Leong, X. Zhao, *Adv. Mater.* **2014**, *26*, 1763.
[7] F. Brau, H. Vandeparre, A. Sabbah, C. Poulard, A. Boudaoud, P. Damman, *Nat. Phys.* **2011**, *7*, 56.
[8] L. Pocivavsek, R. Dellsy, A. Kern, S. Johnson, B. Lin, K. Yee, E. Cerda, *Science* **2008**, *320*, 912.
[9] P. Kim, M. Abkarian, H. A. Stone, *Nat. Mater.* **2011**, *10*, 952.
[10] Y. Cao, J. W. Hutchinson, *J. Appl. Mech.* **2012**. *79*, 031019
[11] Y. Ebata, A. B. Croll, A. J. Crosby, *Soft Matter* **2012**, *8*, 9086.
[12] E. P. Chan, E. J. Smith, R. C. Hayward, A. J. Crosby, *Adv. Mater.* **2008**, *20*, 711.
[13] J. Y. Chung, J. P. Youngblood, C. M. Stafford, *Soft Matter* **2007**, *3*, 1163.
[14] P. C. Lin, S. Yang, *Soft Matter* **2009**, *5*, 1011.
[15] S. G. Lee, H. S. Lim, D. Y. Lee, D. Kwak, K. Cho, *Adv. Funct. Mater.* **2012**, *23*, 547.
[16] C. Badre, J. P. Chapel, S. Yang, *Soft Matter* **2011**, *7*, 9886.
[17] J. Zang, X. Zhao, Y. Cao, J. W. Hutchinson, *J. Mech. Phys. Solids* **2012**, *60*, 1265.
[18] D. Vella, J. Bico, A. Boudaoud, B. Roman, P. M. Reis, *Proc. Natl. Acad. Sci. USA* **2009**, *106*, 10901.
[19] J. Zang, S. Ryu, N. Pugno, Q. Wang, Q. Tu, M. J. Buehler, X. Zhao, *Nat. Mater.* **2013**, *12*, 321.
[20] A. L. Volynskii, S. Bazhenov, O. V. Lebedeva, N. F. Bakeev, *J. Mater. Sci.* **2000**, *35*, 547.
[21] M. Staykova, D. P. Holmes, C. Read, H. A. Stone, *Proc. Natl. Acad. Sci. USA* **2011**, *108*, 9084.
[22] M. Guvendiren, S. Yang, J. A. Burdick, *Adv. Funct. Mater.* **2009**. *19*, 3038.
[23] D. Breid, A. J. Crosby, *Soft Matter* **2011**, *7*, 4490.
[24] D. Breid, A. J. Crosby, *Soft Matter* **2013**, *9*, 3624.
[25] E. Riks, *J. Appl. Mech.* **1972**, *39*, 263.
[26] D. Chen, L. Jin, Z. Suo, R. C. Hayward, *Mater. Horizons* **2014**, *1*, 207.
[27] S. Dabral, J. Van Etten, X. Zhang, C. Apblette, G. Yang, P. Ficalora, J. McDonald, *J. Electron. Mater.* **1992**, *21*, 989.